Proceedings of International Conference on Heat Exchanger Fouling and Cleaning - 2011 (Peer-reviewed)
June 05 - 10, 2011, Crete Island, Greece
Editors: M.R. Malayeri, H. Müller-Steinhagen and A.P. Watkinson
Published online
www.heatexchanger-fouling.com

# DYNAMIC GAUGING OF SOFT FOULING LAYERS ON SOLID AND POROUS SURFACES

**V.Y. Lister[1], W. Augustin[2], Y.M.J Chew[3], P.W. Gordon[1], A.E. Kvarngren[1], M. Mayer[2], W.R. Paterson[1], J.M. Peralta[1,4], S. Scholl[2], P.P. van Uytvanck[1] and D.I. Wilson[1]**

[1] Department of Chemical Engineering and Biotechnology, New Museums Site, Pembroke Street, Cambridge, CB2 3RA, UK
E-mail (diw11@cam.ac.uk)
[2] Technische Universität Braunschweig, Institute for Chemical and Thermal Process Engineering, Langer Kamp 7, 38106 Braunschweig, Germany
[3] Department of Chemical Engineering, Building 9 West, University of Bath, Claverton Down, Bath, BA2 7AY
[4] Instituto de Desarrollo Tecnológico para la Industria Química (INTEC), Universidad Nacional del Litoral - CONICET, Güemes 3450, S3000GLN, Santa Fe, Argentina.

## ABSTRACT

Fluid dynamic gauging allows the thickness of soft foulant layers immersed in liquid to be measured *in situ* and in real time under a range of flow conditions. This paper reports some recent developments of the technique which are likely to be of interest to researchers working in the area of fouling and cleaning.

## INTRODUCTION

The technique of fluid dynamic gauging (FDG) was developed at Cambridge to measure, in situ and in real time, the thickness of soft-solid fouling layers which are otherwise readily deformed on contact with a measurement tool or collapse when removed from their native liquid environments. Since the concept was first demonstrated by Tuladhar *et al*. (2000) for whey protein foulants in a quiescent liquid on a solid surface, FDG has developed to measure the thickness of different materials on a range of surface natures and where the bulk liquid is moving and/or heated. Parallel fluid flow simulations using computational fluid dynamics have allowed the technique to be used to study the strength and deformation behaviour of the fouling layer. A review of these methods is presented by Saikhwan *et al*. (2007).

FDG is based on the pre-existing technique of pneumatic gauging (Macleod *et al*., 1962), wherein the change in the flow rate of air through a conical nozzle as it approached a surface allowed the distance from the surface to be determined, without contacting the surface. FDG employs a liquid as the fluid, usually that in contact with the liquid-rich layer, and works by sucking the liquid into the nozzle. Figure 1 illustrates the concept. A pressure difference is established across the nozzle and this causes liquid to flow into the nozzle. The position of the nozzle relative to the substrate, $h_0$, is measured independently. The mass flow rate, $m$, is usefully sensitive to the clearance, $h$, in the range $0 < h/d_t < 0.25$ and this allows $h$ to be calculated. The thickness of the layer, $\delta$, is then estimated from $\delta = h_0 - h$. Developments of the gauge have included computer control and scanning capability which allow measurements to be made automatically, at several locations in sequence, with an accuracy of ±5 μm (Gordon *et al*., 2010a). This paper reports some recent developments of the technique to extend its range of applications.

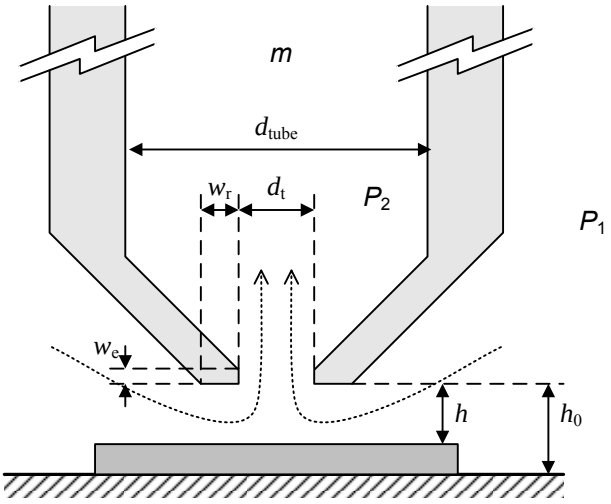


Fig. 1 Schematic of an FDG nozzle. The nozzle angle, here 45°, and dimensions $d_{tube}$, $d_t$, $w_e$ and $w_r$ are design parameters.

## PRESSURE MODE GAUGING

FDG measurements are based on knowledge of the relationship between the flow rate and clearance, which Tuladar *et al*. (2000) reported in dimensionless terms as

$$C_d = f\left(\frac{h}{d_t}, \frac{w_r}{d_t}, Re_t\right) \qquad [1]$$

Here, $Re_t$ is the Reynolds number defined at the nozzle throat. $C_d$ is a dimensionless flow rate, defined as

$$C_d \equiv \frac{\text{actual mass flow rate}}{\text{ideal mass flow rate}} = \frac{4m}{\pi d_t^2} \frac{1}{\sqrt{2\rho(P_1 - P_2)}} \qquad [2]$$

where $P_1$ and $P_2$ are the pressures upstream and downstream of the nozzle, respectively.

Tuladhar *et al*. showed that the $h/d_t$ contribution to $C_d$ in equation [1] was the dominant influence over the range of interest. Their data were collected under conditions of fixed pressure driving force, such that $P_1$-$P_2$ was approximately constant. When making FDG measurements, the mass flow rate is converted to $C_d$ using equation [2], and $h$ can then be calculated. This method of measurement is termed *mass flow mode* and works well when the pressure differences required are manageable and the flow rate is allowed to vary. Figure 2 shows a set of data obtained under this mode.

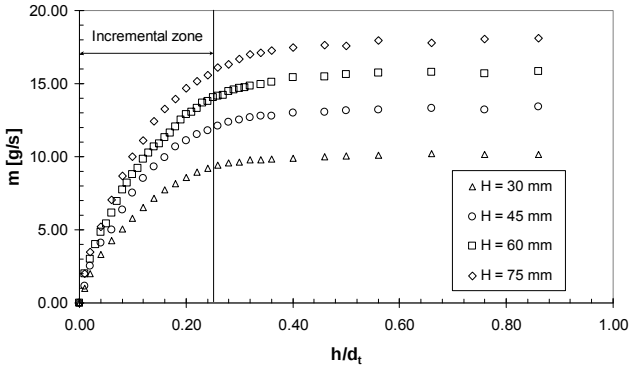


Figure 2: Flow-clearance characteristic of FDG operation in mass flow mode on a filter paper surface. Liquid – water at 18°C. $H$ values denote the overall pressure driving force.

Inspection of equation [2] suggests a second mode of operation, namely one where the mass flow rate is held approximately constant (and measured) and the pressure drop is measured as the nozzle is moved towards the fouling layer. $C_d$ decreases as $h/d_t$ approaches zero, indicating that $P_1$-$P_2$ should increase. We term this *pressure mode gauging*. It offers advantages in (*i*) specifying the mass flow rate, potentially reducing the volume of liquid removed and maintaining constant bulk conditions in a duct flow; (*ii*) decoupling the measurement from the absolute pressure, allowing measurements to be made at both low and high pressure; and (*iii*) permitting recycling of the liquid back to the system, reducing the volume of liquid required or simplifying studies involving reacting or biological species.

Figure 3 shows sets of data collected using this mode on a flat metal plate serving as the base of a 15×15 mm duct in the presence of a bulk flow. The pressure drop across the gauge nozzle in Figure 3(a) can be seen to be independent of bulk flow rate. The latter is reported in terms of duct Reynolds number, $Re_{duct} = u_m L/\nu$, where $u_m$ is the mean velocity in the duct, $L$ the wall length and $\nu$ the kinematic viscosity. The corresponding $C_d$ – $h/d_t$ profiles in Figure 3(*b*) are of the same form as seen in the mass flow mode (*e.g*. Figure 2) and are independent of $Re_{duct}$. Gu *et al*. (2009) reported mass flow mode measurements for this configuration, and their $C_d$ – $h/d_t$ profiles show good agreement with those in Figure 3(*b*) (data not reported).

Pressure mode gauging differs from flow mode in requiring a sensitive differential pressure transducer in addition to an accurate flow meter. The resolution of the $h/d_t$ measurements for the two modes is similar, here ±10 μm for a nozzle with $d_t$ = 1 mm and shape in Figure 1.

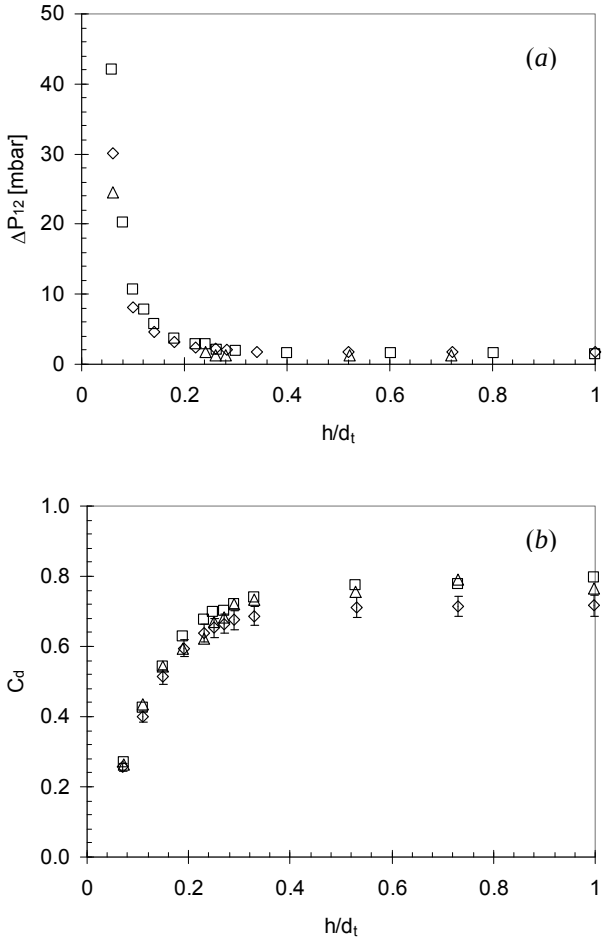


Figure 3 Pressure mode FDG calibration plots for gauging on a metal plate in a duct flow system. Conditions: $m$ ~ 0.37 g s$^{-1}$, $P_{static}$ (125-140 mbar), different bulk flow rates. Symbols: triangles $Re_{duct}$ = 450; squares $Re_{duct}$ = 650; diamonds $Re_{duct}$ = 1090. Reproduced from Lister *et al*. (2010).

Gu *et al*. (2011) demonstrated that pressure mode gauging can be used to make thickness measurements in annular configurations. This geometry is important for fouling test systems such as the HTRI fouling probe and 'cold fingers' used in wax deposition testing, where liquid is passed over a heated (or cooled) central rod. Gu *et al*. showed that both pressure mode and mass flow mode gauging could be performed on the inner tube surface in flowing liquids for two different geometries, namely (*i*) $d_{outer}$ = 35 mm, $d_{inner}$ = 21 mm, $90 < Re_{duct} < 29{,}000$, and (*ii*) $d_{outer}$ = 30 mm, $d_{inner}$ = 12 mm $250 < Re_{duct} < 10{,}000$. They also showed that FDG measurements could be made reliably on a heated rod (apparatus (*ii*)), confirming that pressure mode gauging can be used to measure changes in deposit thickness. The advantage of pressure mode gauging in this configuration is the ability to control the amount of liquid withdrawn, and freedom to operate at higher pressures. A sensor based on pressure mode gauging is

currently being commissioned for use on the HIPOR testing facility at Imperial College, London.

Lister *et al*. (2010) demonstrated that pressure mode gauging can also be applied to porous surfaces such as membranes. They were able to track the development of particulate fouling layers growing on a microfiltration membrane during cross-flow filtration of a dilute suspension in the laminar regime. Jones *et al*. (2011) similarly employed pressure mode gauging to study the build-up of fouling layers on ultrafiltration membranes during cross-flow filtration of sugar molasses operating at transmembrane pressures of up to 1 bar and bulk velocities up to 2.9 m $s^{-1}$ *i.e.* in the turbulent regime. Figure 4 shows some of the real time fouling data generated in their study.

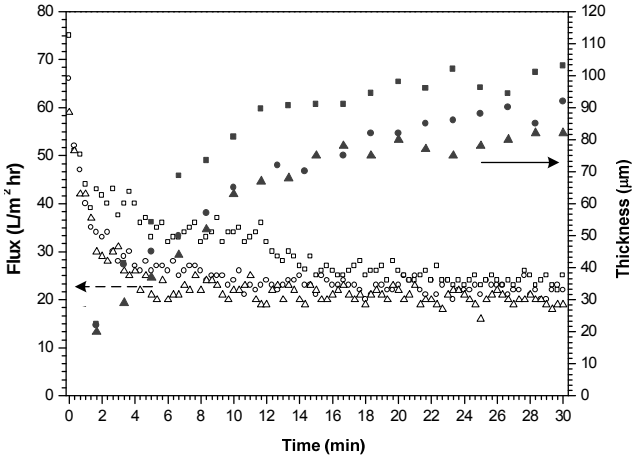


Figure 4 Application of pressure mode gauging to membrane fouling. Effect of TMP on deposit build-up and permeate flux over time. Solid symbols - cake layer thickness (right abscissa); open symbols - permeate flux (left abscissa) . TMP values: ■ - 1 bar, ● - 0.55 bar, ▲ - 0.35 bar. $Re_{duct}$ = 9820, 21.5 ºC. Reproduced from Jones *et al*. (2010).

## SCANNING SOFT SURFACES

Gordon *et al.* (2010a) reported the development of a scanning FDG (sFDG) sensor, which could be moved across a surface and measure clearances, *h*, with a measurement thickness accuracy of ±5 μm. This device operates in mass flow mode under computer control. Its versatility has been increased by the following modifications:

### Sweeping

A reservoir system for the test liquid has been added to control the composition and temperature of test liquid. These can then be manipulated as desired, allowing the effect of pH, ionic strength or temperature on deposit behaviour to be assessed. By sweeping across a parameter range, conditions causing noteworthy changes can be identified for further, detailed study.

Figure 5 shows an example of results obtained for the swelling of gelatin. The pH was increased in steps of ~ 0.3 pH units at 10 min intervals by adding 0.1 M or 0.2 M NaOH solution. The film shrinks initially due to the shielding of charges on the protein, reducing intermolecular repulsion, as the ionic strength of the solution increases. Around pH 10.5 the film starts to swell owing to deprotonation of proline and hydroxyproline, two of the amino acids in gelatine. Their p$K_a$ value is marked by a vertical dashed line on the plot. Separate experiments using solutions with different NaOH concentrations show good agreement up to pH 11. Better agreement at high pH would be obtained by allowing longer times for steady state to be reached.

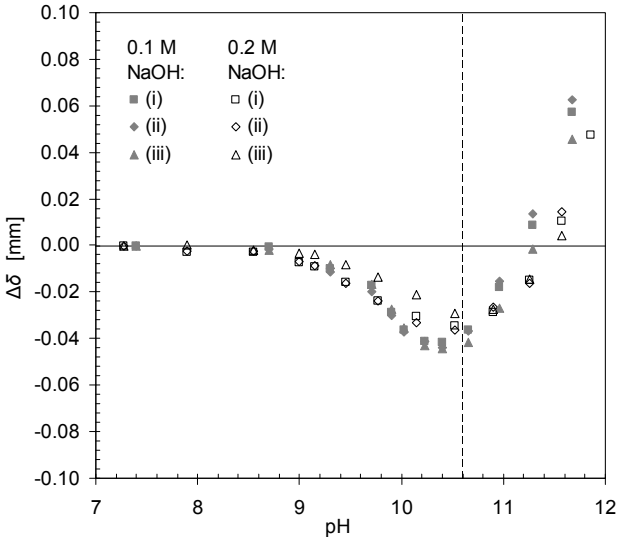


Figure 5 pH sweep testing of gelatine film swelling in the sFDG system. $\Delta\delta$ is the change in film thickness. Labels (*i*) to (*iii*) denote three points on the deposit surface 5 mm apart. Conditions: 80 μm film pre-swollen in reverse osmosis water at 20ºC, pH 6.77. Reproduced from Gordon *et al*. (2010b).

### Softer films: biofilms

Addition of a computer controlled discharge arm allows the pressure driving force, $P_1$-$P_2$, to be adjusted on demand. Since the gauging flow rate, and the shear stress imposed on the surface (or layer), is directly related to $P_1$-$P_2$ (see equations (1) and (2)), this allows the deformation behaviour of a layer to be studied. Initially the nozzle is operated using a low flow rate to locate the surface. With the nozzle position fixed, the pressure driving force is increased for a period and then returned to the low flow rate and *h* measured. Changes in *h* correspond to changes in layer thickness. The scanning capability means that this test can be performed at different locations and a statistically useful number of measurements collected from a single sample.

This tool also allows softer fouling layers to be studied. Biofilms represent an important example of such materials, occurring in water treatment bioreactors, heat exchanger biofouling, and also in the form of algal biofilms for biofuel manufacture. Möhle *et al*. (2007) employed single point FDG measurement in combination with scanning laser confocal microscopy to study activated sludge biofilms and

reported cohesive strengths of ~ 6-8 Pa and the presence of a stable base biofilm which was not removed by gauging.

The sFDG has been used recently to look at thin biofilms such as those employed in photovoltaic applications (McCormick *et al*., 2011). The photograph of the cyanobacterial biofilm in Figure 6 conveys the uneven topography of such layers and the need to scan at several points in order to accumulate representative data sets. Figure 7 shows the results obtained for two biofilms generated using different bacteria on similar substrates. Measurements were performed with the nozzle approaching the biofilm for a short period then moved to another point. The influence of prolonged shear could be investigated if desired.

Figure 6 Gauging of a *Synechococcus* biofilm grown on perspex. Nozzle tube external diameter 6 mm.

Figure 8 shows the results obtained for strength testing of an algal (*Chlorella*) biofilm grown on frosted glass. The shear stress imposed on the biofilm was estimated using the method reported in Gordon *et al*. (2010b). The data sets collected at different locations show good agreement.

The biofilm thickness initially decreases steadily from its starting value of 120-140 μm as the shear stress increases, corresponding to cohesive breakdown. Catastrophic failure occurs at a stress of 20-25 Pa, which was accompanied by visual observation of detachment of material from the surface. A thin layer of residual material may reside on the surface, but this could not be reliably gauged using this version of the sFDG.

(*a*)

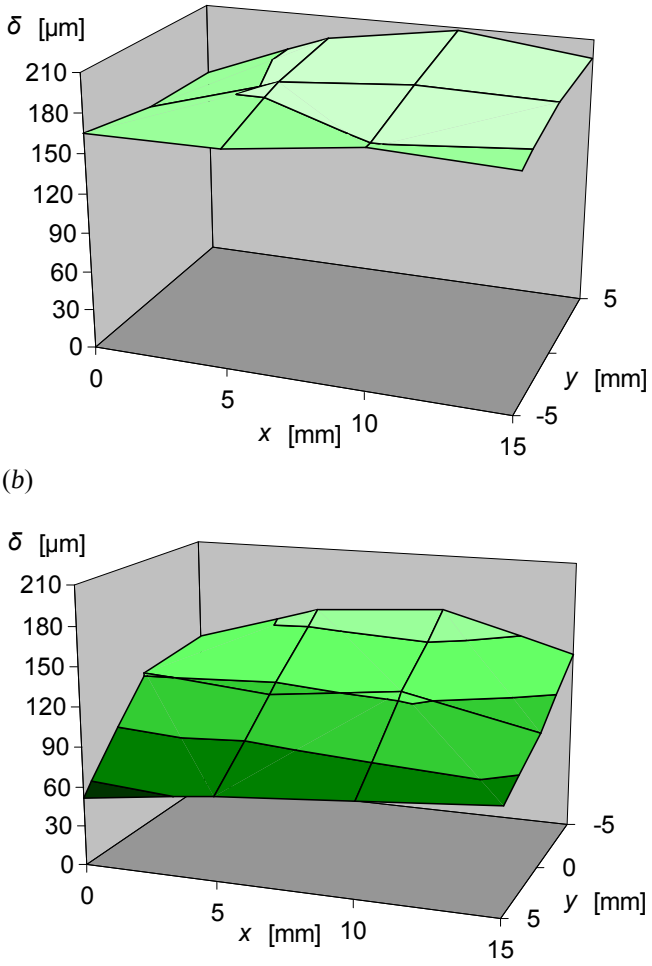


Figure 7 sFDG scans of biofilm thickness for (*a*) *Synechococcus* (cyanobacterium) and (*b*) *Chlorella*, an algal strain, both grown on polyethelene terephthalate (PET) films coated with a layer of indium tin oxide. Resolution ±10 μm: *x* and *y* are the co-ordinates on the substrate surface. Contours in z are separated by 30 μm.

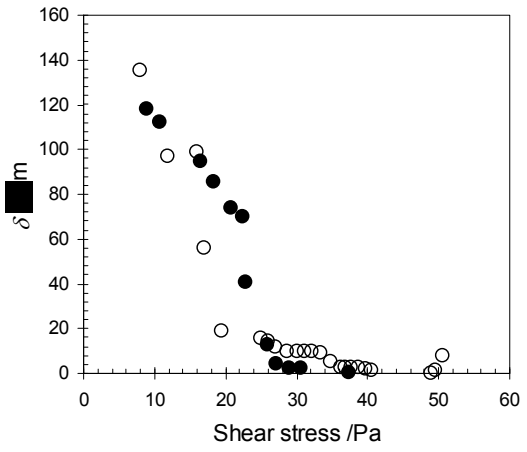


Figure 8 sFDG strength testing of *Chlorella* biofilm grown on a frosted glass substrate. Data collected at two locations. Resolution in $\delta$ measurements ±10 μm.

Refinements of the device, including combining the FDG measurements with a confocal microscope to allow the biofilm to be studied *in situ*, as described for whey protein films by Saikhwan *et al*. (2007), are currently being pursued. The scope to study the influence of biofilm growth conditions, age, surface nature and biofouling in combination with other deposition mechanisms is large.

## SCANNING SEVERAL SURFACES

The ability to make measurements at several locations can also be exploited to compare different surface treatments in a single test. Conventional testing regimens (*e.g*. Geddert *et al*., 2011) involve repeating tests with different surfaces, creating potential for random and systematic errors between experiments. sFDG testing allows several surfaces to be compared in a single experiment by using patterned plates such as those shown in Figure 9. Deposit layers can be generated from the same batch of material and the influence of surface treatment on fouling compared directly in a single experiment. Likewise, the response of a deposit or coating on each surface to a given cleaning solution or cleaning regimen can be compared directly.

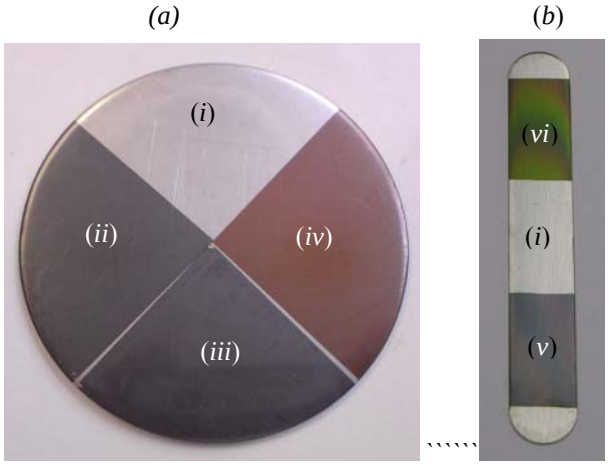


Figure 9 Stainless steel 316 plates coated with different substrates for sFDG testing. (*a*) 50 mm diameter disc, marked regions (*i*) control, 316SS; (*ii*) SiCON®; (*iii*) SiCAN and (*iv*) DLC; (*b*) 25 mm × 150 mm strips, (*v*) SiCAN and (*vi*) SiCON®. Coating performed by Fraunhofer Institute for Surface Engineering and Thin Films IST, Braunschweig.

The value of parallel testing is demonstrated by the results for removal of a starch deposit in Figure 10. Stainless steel discs similar to those in Figure 9(*a*) were prepared with smooth (*Ra* = 0.071 μm) or deliberately roughened surfaces. Sandblasting gave *Ra* = 1.584 μm while grade P120 sandpaper gave *Ra* = 0.387 μm). Water contact angle measurements showed an increase in average value from 67º for the polished steel to 90º and 91º for the sandpaper and sandblasted surfaces, respectively. Starch deposits were generated using a protocol based on that reported by Schöler *et al*. (2011), giving an average thickness of 15-40 μm. Their removal by soaking in reverse osmosis water was studied at 20ºC.

The cleaning profiles in Figure 10 show the same general trend, of rapid swelling, followed in some cases by a period of steady thickness, before rapid removal to leave a residual layer. The extent of swelling and length of the steady period varies noticeably. Comparison of the profiles for the notionally identical smooth surfaces emphasizes the random nature of this coating. In the absence of sFDG testing, the variation between coatings would make comparisons between the different surface treatments difficult and require many tests in order to generate statistically useful results.

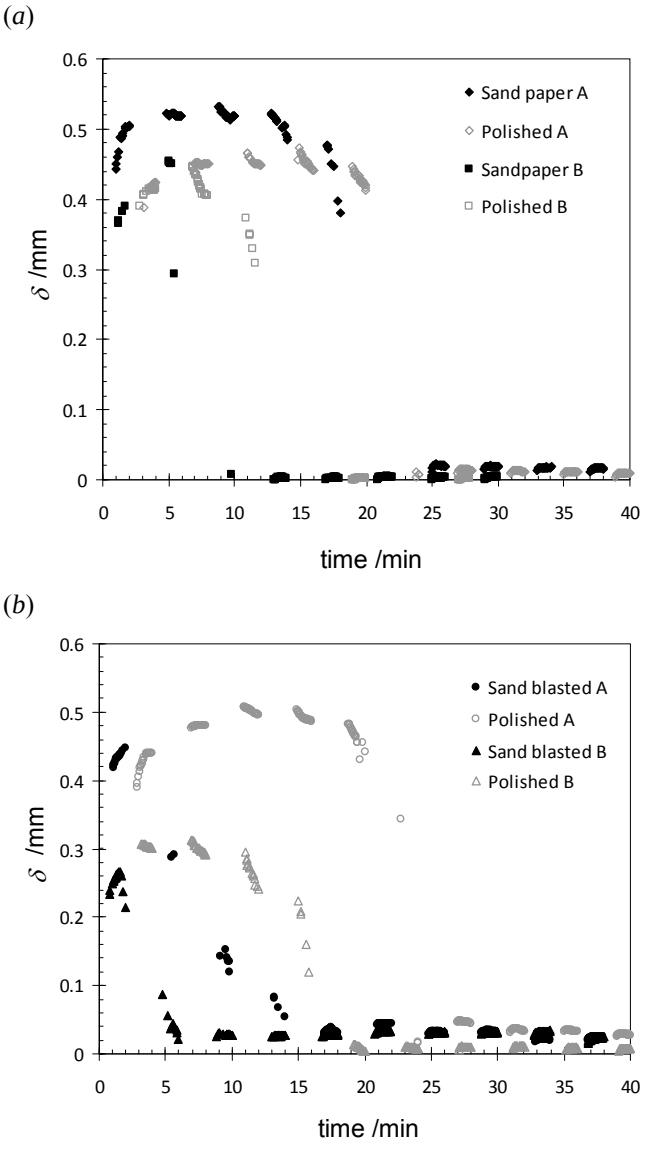


Figure 10 sFDG testing of removal of starch deposits from roughened and smooth 316 stainless steel plates in reverse osmosis water at 20ºC. Symbols indicate data collected in the same test.

SFDG testing, however, allows the surfaces to be compared directly. In most cases the rate and extent of swelling is the same on both surfaces, which is expected as

this is a deposit chemistry response. The roughened surfaces, however, consistently release the deposit before the polished one, with the sandblasted surface releasing the deposit almost as soon as swelling had stopped. The smooth surfaces in this case take consistently longer to clean Such observations allow the cleaning mechanism to be elucidated. Further testing using commercial coatings (Figure 9) with heat-induced deposits (as opposed to dried-on coatings) is under way.

## NOZZLE DEVELOPMENT

The simple conical geometry of nozzles employed in FDG studies, such as that shown in Figure 1, are based on those used previously for pneumatic gauging. The conical internal configuration is key to the operation of the device as this geometry, coupled with the radial flow of liquid into the nozzle, concentrates the pressure drop at the nozzle tip. In contrast, Deshpande and Vaishnav (1982) employed simple capillaries to study surface deformation of tissue samples. The external nozzle shape determines the flow pattern between the nozzle and the surface being studied, and therefore the stresses imposed on the layer. There is therefore scope to improve the sensitivity of the gauging measurement, *i.e*. by extending the size of the incremental zone beyond $h/d_t \sim 0.25$, or to impose a more uniform shear stress profile on the substrate.

Direct measurement of the shear stress imposed by a fluid flow on a surface is challenging, and most methods rely on measurement of another parameter. Measurement of the absolute pressure distribution is relatively simple and can be directly related to predictions of the flow field obtained from computational fluid dynamics (CFD) simulation (Chew *et al*., 2004). CFD simulations offer reliable predictions for FDG in quasi-stagnant flows (where the only flow is that associated with the gauge) on permeable and impermeable surfaces, as the flow is generally in the creeping or laminar (inertial) regime. At higher Reynolds numbers, the transition to more complex flow patterns renders CFD predictions less reliable without detailed experimental studies. Gu *et al.* (2009) obtained reasonable agreement between measured and predicted pressures for FDG in duct flows with $Re_{duct}$ up to ~500. Estimation of shear stresses at higher duct flow Reynolds numbers would require considerable computational effort, guided by physical insight. The design of nozzles is therefore aimed at applications in quasi-stagnant and relatively slow duct flows.

In principle it should be possible to design a nozzle shape *in silico* and test it using CFD simulations. Experimental verification is nevertheless required to confirm the reliability of the code. Figure 10(*a*) compares measurements of the pressure measured on the axis of symmetry of a $d_t$ = 5 mm conical gauging nozzle, with shape shown in Figure 10(*b*), at different values of $h$ with the predictions of a CFD simulation reported by Peralta *et al*. (2011a). Similarly good agreement is evident between the measured and predicted radial distribution of pressure for two different values of $h/d_t$ in Figure 10(*b*).

CFD methods are most useful in assessing candidate geometries and are relatively inefficient for actually generating the candidates. Peralta *et al*. (2011a) compared the radial distribution of surface shear stress generated by convergent, divergent and toroidal external nozzle shapes. These indicated that a uniform shear stress distribution could be achieved under certain combinations of geometry and flow conditions. They extended this approach by developing an analytical model of the flow between a horizontal surface and a gauging nozzle of arbitrary shape based on the lubrication approximation.

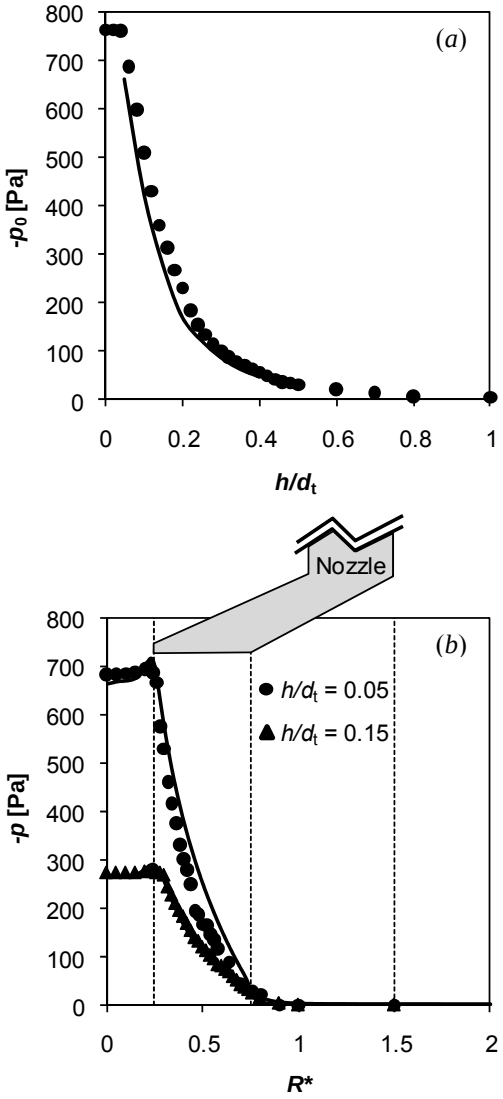


Figure 10 Comparison of measured pressure exerted on a solid surface beneath a $d_t$ = 5 mm gauge with CFD simulations. (*a*) Effect of clearance, $h/d_t$, on pressure at stagnation point, dimensionless radial coordinate $R^* = 2r/d_{tube} = 0$. (*b*) pressure distribution in radial direction. Nozzle shape indicated in (*b*): vertical dashed lines show location of vertices on external surface. Reproduced from Peralta *et al*. (2011a).

Figure 11 shows one of their results, where the surface shear stress distribution was specified to be (*i*) uniform between dimensionless radial position $0.17 \le \tilde{r}' \le 0.58$, and (*ii*) decay gradually ($\tau_w \propto \tilde{r}'^{-1}$) between $0.58 < \tilde{r}' \le 1.0$. The Figure shows the nozzle shape required to obtain the specified shear stress distribution. Here, the dimensionless clearance $\tilde{h} \equiv h/h_o$, where $h_o$ is the clearance between the external part of the nozzle and the gauged surface at the outer radius, $r_o$. Similarly, $\tilde{r} \equiv r/r_o$. For this case, $\tilde{h} \propto \tilde{r}'^{-½}$ in the inner zone and $\tilde{h} = 1$ in the outer zone.

The agreement between the CFD prediction of the surface shear stress distribution and the specified form is excellent. It is noteworthy that the shear stress exerted on the surface is predicted to be ~0.3 Pa, which is suited for softer fouling layers. Further work in this area includes local velocimetry studies of the flow fields. This work indicates that it is possible to identify nozzle shapes for specific gauging applications.

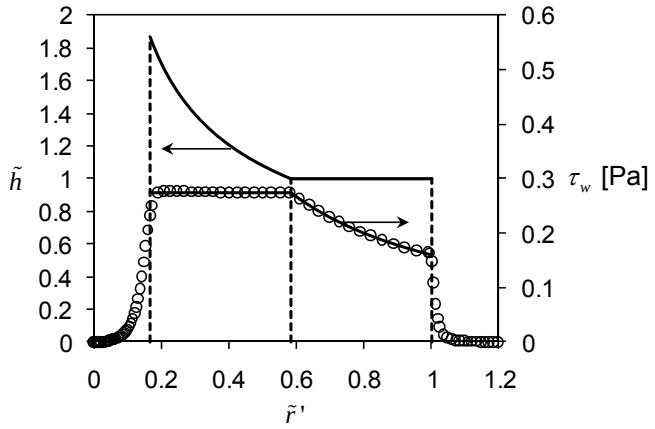


Figure 11. FDG nozzle shape designed using the analytical approach described by Peralta *et al*. (2011). The shear stress profile is specified and the shape, expressed in terms of dimensionless clearance, $\tilde{h}$, determined. Loci show the specified shear stress distribution and geometry. The shape was then used in a CFD simulation of the flow and the predicted shear stress distribution is plotted as the open circles.

## CONCLUSIONS

Fluid dynamic gauging allows experimenters to monitor the thickness of soft coating layers immersed in stagnant or flowing liquids. Recent developments in the technique reported here which are relevant to researchers working on fouling or cleaning are:

1. Development of pressure mode gauging, which allows measurements to be made independent of absolute pressure and at controlled liquid removal rates. This is particularly useful for studies in pressurized flows, and can be applied to membranes.
2. Enhancement of the scanning FDG technique, allowing tests to be performed with varying liquid parameters such as temperature or composition.
3. Application of scanning FDG to soft layers such as biofilms, which exhibit variations in deposit thickness and, thereby allowing statistical data to be generated.
4. Comparative, concurrent testing of different surfaces.
5. Rigorous mathematical modelling of FDG performance based on the lubrication approximation, that relate the nozzle geometry with specific flow variables (*i.e.* $\tau_w$, $p$, etc) and/or optimal states of operation of the nozzle. These models are simple and easy to be implemented for screening of potential nozzle shape configurations.

## NOMENCLATURE

### Roman

| | |
|---|---|
| $C_d$ | discharge coefficient, - |
| $d_t$ | throat diameter, m |
| $d_{tube}$ | tube diameter, m |
| $h$, $h_o$ | clearance, initial value, m |
| $\tilde{h}$ | dimensionless clearance, - |
| $L$ | duct wall length, m |
| $m$ | mass flow rate, kg $s^{-1}$ |
| $P_i$ | pressure at location *i*, Pa |
| $P_{static}$ | static pressure, Pa |
| $R^*$ | dimensionless radial position, - |
| $Ra$ | average absolute roughness, m |
| $\tilde{r}'$ | dimensionless radial position, - |
| $Re_t$ | Reynolds number at throat, - |
| $Re_{duct}$ | Reynolds number, duct, - |
| TMP | transmembrane pressure, Pa |
| $u_m$ | bulk mean velocity, m $s^{-1}$ |
| $w_e$ | nozzle edge length, m |
| $w_r$ | rim width, m |
| $x$, $y$ | co-ordinates in horizontal plane |

### Greek

| | |
|---|---|
| $\delta$ | deposit thickness, m |
| $R^*$ | density, kg $m^{-3}$ |
| $\tau_w$ | wall shear stress, Pa |

## ACKNOWLEDGEMENTS

We wish to acknowledge the skill and creative contributions made by Lee Pratt, Andy Hubbard, Gary Chapman, Karl Karrenführer and Surinder Sall in designing and fabricating the various FDG devices. The biofilms were supplied by Alistair McCormick. Several parts of the work reported here were investigated as part of a British Council/DAAD Collaboration between the groups at TU-BS and Cambridge. A CONICET Visiting Fellowship for JMP is gratefully acknowledged.

**REFERENCES**

Y.M.J. Chew, W.R. Paterson and D.I. Wilson, 2004, Dynamic gauging for measuring the strength of soft deposits, *J. Food Eng*, Vol. 65(2), 175-187.

M.D. Deshpande and R.N. Vaishnav, 1982, Submerged laminar jet impingement on a plane, *J. Fluid Mechanics*, Vol. 114, 216-236.

T. Geddert, W. Augustin and S. Scholl, 2011, Influence of surface defects and aging of coated surfaces on fouling behaviour, *Heat Transfer Engineering*, Vol. 32(3-4), 300-306.

P.W. Gordon, A.D. Brooker, Y.M.J. Chew, D.I. Wilson and D.W. York, 2010a, A scanning fluid dynamic gauging technique for probing surface layers, *Measurement Sci. Tech*., Vol. 21, 085103.

P.W. Gordon, A.D.M. Brooker, Y.M.J. Chew, D.I. Wilson and D.W. York, 2010b, Studies into the swelling of gelatine films using a scanning fluid dynamic gauge, *Food & Bioproducts Proc*., Vol. 88, 357-364.

T. Gu, Y.M.J. Chew, W.R. Paterson and D.I. Wilson, 2009, Experimental and CFD studies of fluid dynamic gauging in duct flows, *Chem. Eng. Sci.,* Vol. 64, 219-227.

T. Gu, F. Albert, W. Augustin, Y.M.J. Chew, M. Mayer, W.R.P. Paterson, S. Scholl, I. Sheikh, K. Wang and D.I. Wilson, 2011, Application of fluid dynamic gauging to annular test apparatuses for studying fouling and cleaning, *Exptl. Thermal Fluid Sci.,* Vol. 35, 509-520.

S.A. Jones, Y.M.J. Chew, M.R. Bird and D.I. Wilson, 2010, The application of fluid dynamic gauging in the investigation of synthetic membrane fouling phenomena, *Food & Bioproducts Proc*., Vol. 88, 409-418.

V.Y. Lister, C. Lucas, P.W. Gordon, Y.M.J. Chew and D.I. Wilson, 2010, Pressure mode fluid dynamic gauging for studying cake build-up in cross-flow microfiltration, *J. Membrane Sci.,* Vol. 366, 304-313.

A.J. McCormick, P. Bombelli, A.M. Scott, A.J. Philips, A.G. Smith, A.C. Fisher, C.J. Howe, 2011, Photosynthetic biofilms in pure culture harness solar energy in a mediatorless bio-photovoltaic cell (BPV) system, submitted to *Energ. Environ. Sci*.

R.B. Möhle, T. Langemann, M. Haesner, W. Augustin, S. Scholl, T.R. Neu, D.C. Hempel and H. Horn, 2007, Structure and shear strength of microbial biofilms as determined with confocal laser scanning microscopy and fluid dynamic gauging using a novel rotating disc biofilm reactor, *Biotech Bioeng*, Vol. 98(4), 747-754.

N. Macleod, M.D. Cox and R.B. Todd, 1962, A profilometric technique for determining local mass transfer rates – Application to the estimation of local heat-transfer coefficients in a nuclear reactor. *Chem. Eng. Sci.,* Vol. 17, 923-935.

J.M. Peralta, Y.M.J. Chew and D.I. Wilson, 2011a, Effect of nozzle external geometry on the pressure and shear stress exerted on the surface being gauged in fluid dynamic gauging, *Chem. Eng. Res. Des*. in press.

J.M. Peralta, Y.M.J. Chew and D.I. Wilson, D.I., 2011b, An analytical method for selecting the optimal nozzle external geometry for fluid dynamic gauging, *Chem. Eng. Sci*., Vol. 66, 3579–3591.

P. Saikhwan, Y.M.J. Chew, W.R. Paterson and D.I. Wilson, 2007, Fluid dynamic gauging: a technique for studying the cleaning of food process surfaces, *Food Manufacturing Efficiency*, Vol. 1(2), 35-41.

M. Schöler, P.W. Gordon, H. Föste, M. Mauermann, Y.M.J. Chew, W. Augustin, S. Scholl, D.I. Wilson, J.P. Majschak, Influence of surface topography of cohesive soil layers on their removal kinetics in CIP processes, *Proc*. Heat Exchanger Fouling and Cleaning 9, Fodele Beach, Crete, June 2011.

T.R. Tuladhar, W.R. Paterson, N. Macleod and D.I. Wilson, 2000, Development of a novel non-contact proximity gauge for thickness measurement of soft deposits and its application in fouling studies, *Can. J. Chem. Eng*., Vol. 78, 935-947.